Chapter 4. Optimum Copper Filter Design

4.1 Requirement Specification

4.1.1 Overview

In theory, a dual-energy radiograph can be used to identify effective atomic number of a given material (using Equation (2.17)). But in practice, there are several major problems. One problem is that Equation (2.17) is true for a particular x-ray energy level, whereas all the dual-energy systems available today use x-ray sources that are polychromatic; that is, they emit x-rays over the whole energy range from zero to the peak voltage on the tube. Figure 4.1-1 shows the output energy spectral distribution of the photons produced by a x-ray tube at both 145 keV, defined as $I_{145}(E)$, and 75 keV, defined as $I_{75}(E)$. This figure was obtained using the MCNP (Monte Carlo N-Particle) software [LOS93] with the prototype scanner model discussed in Chapter 3, and is normalized with a constant. To obtain estimates of R using polychromatic sources, several techniques have been used. These techniques include the following:

- Varying the input energy of the x-ray tube [EUR96], using two scans and one detector for two transmission images;

- Filtering the x-ray energy at the source or the sensor [EIL92], using two scans and one detector for two transmission images;
- Using multiple sensors that have different spectral responses [MIC93], one scan and two detectors for two transmission images.

A true dual-energy system obtains images at two distinct x-ray energies by varying the input energy to x-ray tube, and other systems are called pseudo dual-energy.

Strictly speaking, 145 keV and 75 keV in Figure 4.1-1 refer to the applied input voltages on the x-ray tube, rather than x-rays with energies at 145 keV and 75 keV. But for convenience, we do not always use "the applied input voltage" when we discuss images scanned at high energy and low energy.

The prototype scanning system in the SDAL is required to collect dual-energy images. But it only has one x-ray source and one transmission detector. So two methodologies are proposed,

(i) An optimum copper filter thickness has been selected for high-energy transmission images. Since the spectral response of the x-ray sensors are fixed, the prototype system uses a combination of varying the input energy to the x-ray tube and filtering x-ray energy at the source to obtain images for different energy levels.

(ii) A numerical optimization method has been developed to analyze dual-energy signals. This method estimates the received signals at two distinct energies. The numerical method developed for dual-energy analysis will be given in Chapter 5.

The following sections of this chapter are going to address the choice of the copper filter thickness. A block diagram of design is shown in Figure 4.1-2. It includes: 1) mathematical description of aforementioned problem; 2) design specification; 3) the spectra with different

copper filter thicknesses, which form a collection of the design data, are simulated with MCNP. The prototype scanner model discussed in Chapter 3 will be used in MCNP simulation; 4) design subject to the selection of weights; and 5) evaluation.

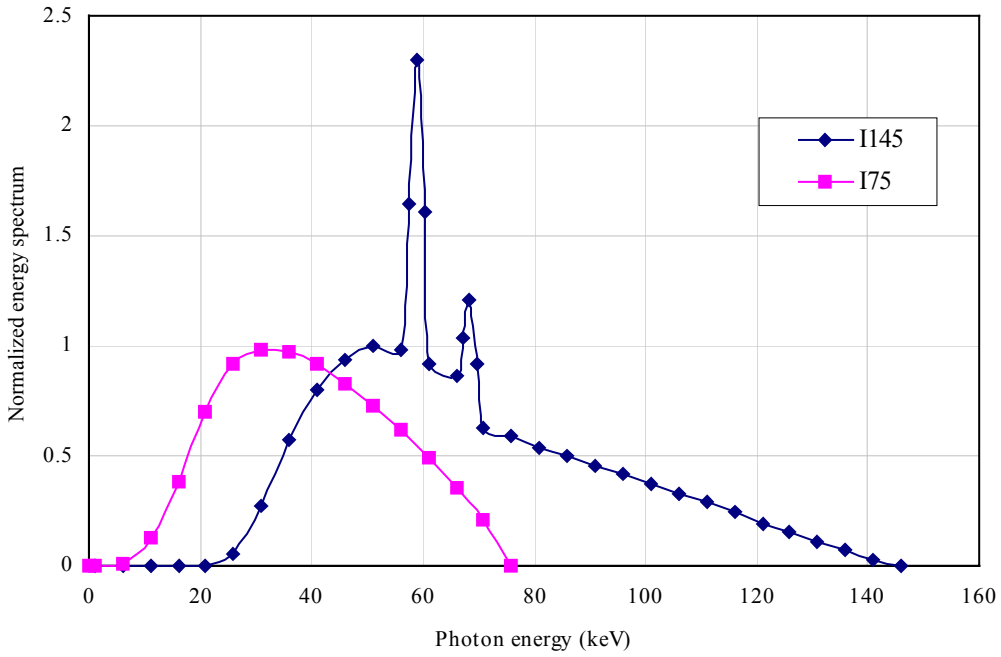

Figure 4.1-1 Energy spectrum of x-ray tube obtained by MCNP.

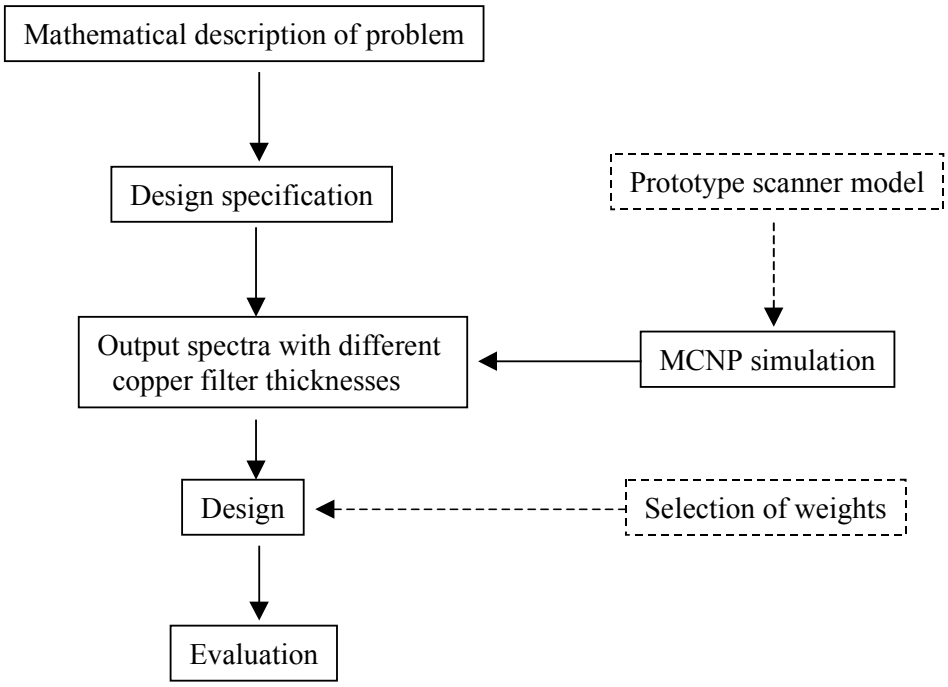

Figure 4.1-2 Block diagram of the copper filter design approach.

4.1.2 Definition of optimum copper filter design

For a given beam current, the total output energy produced by the source is given by the following equation:

$$E_{total} = \int_0^\infty I_0(E)dE\,. \tag{4.1}$$

As seen from Figure 4.1-1, there are two problems with this dual-energy x-ray source. The first one is that the total output energy for the 145 keV signal is significantly higher than for the 75 keV signal. The difference will degrade the performance when only one group of detectors is used. The second problem is that there is significant overlap between the two spectra. Obviously, more overlap between high energy and low energy spectra reduces the ability to extract dual-energy information. In the extreme case, a dual-energy x-ray system will degenerate to a conventional x-ray system if one spectrum overlaps the other completely.

To address these problems, a copper filter is used to attenuate the high energy signal. This is intended to separate the two output energy spectral distributions and balance the total output energy at the two different x-ray tube energy levels. The optimum filter would satisfy the following equations:

$$\int_0^\infty I_L(E)dE = \int_0^\infty I_H(E)dE \tag{4.2}$$

$$\int_0^\infty I_L(E)\,I_H(E)dE = 0 \tag{4.3}$$

where $I_L(E)$ and $I_H(E)$ represent the energy spectra at low and high energy levels in the general case. An explanation of spectrum overlap and signal unbalance is shown in Figure 4.1-3.

To meet the requirement of Equation (4.3), we know that a filter has to be used when materials are scanned at high energy levels. This filter must be thick enough to filter all x-rays below the low energy, i.e., all x-rays below 75 keV in our example. Since the filter would also absorb the x-rays of the higher energy in the mean time when it holds back the x-rays of lower energy, the high energy applied have to be lifted up to keep the requirement for the Equation (4.2). For practical x-ray systems, the design subjects to a constraint on high energy available. So a major design consideration left to us only is the thickness of the copper filter.

Because of practical considerations, it is not possible to satisfy both constraints. To determine an optimum compromise, a cost function is created as follows,

$$C(t) = C_1 \cdot \left[\int_0^\infty I_L(E)dE - \int_0^\infty I_{H,t}(E)dE \right]^2 + C_2 \cdot \int_0^\infty I_{H,t}(E) I_L(E) dE \tag{4.4}$$

where C_1 and C_2 are weighting factors to balance the output signals and spectrum overlap respectively, and $I_{H,t}(E)$ represents the high energy spectrum with a copper filter of thickness t. The goal is to select a thickness t that minimizes Equation (4.4). To realize this goal, the filtered x-ray source spectra at high energy must be simulated first.

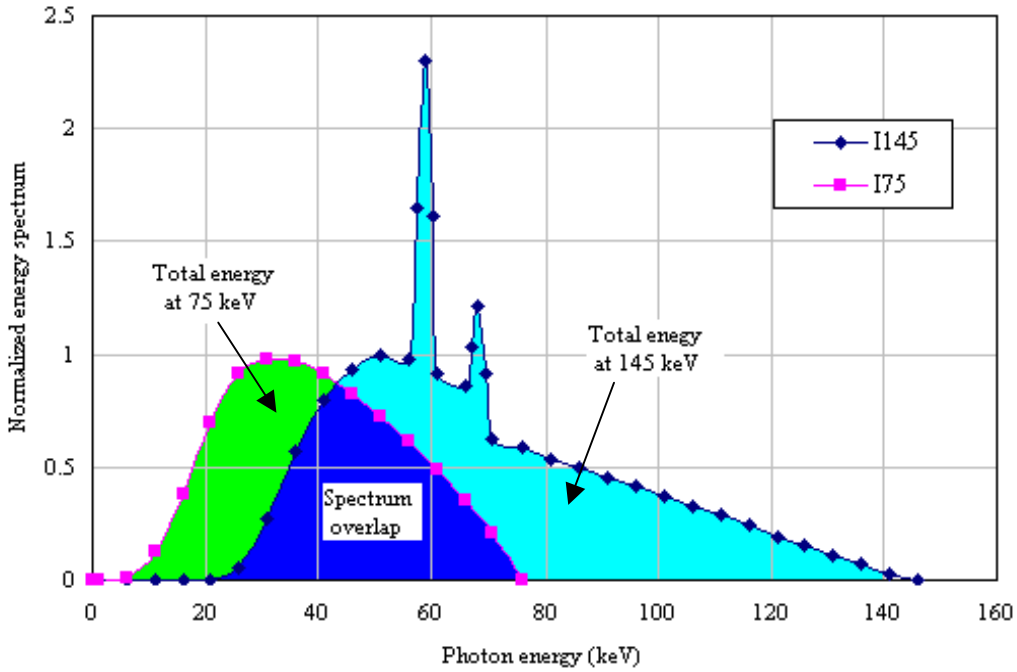

Figure 4.1-3 Explanation of spectrum overlap and signal unbalance.

4.2 MCNP: Method of Solution

MCNP (Monte Carlo N-Particle) [LOS93], a software package developed by Transport Methods Group at Los Alamos National Laboratory to simulate neutron-photon-electron transport through matter, provides us a good method to get the desired data for optimum copper filter design.

The Monte Carlo method is a numerical method of solving mathematical problems by the simulation of random variables [SOB94]. The method enables simulation by any process whose development is influenced by random factors, and it enables us to artificially construct a probabilistic model for many difficult problems.

MCNP treats an arbitrary three-dimensional configuration of materials in geometric cells bounded by first- and second-degree surfaces and some special fourth-degree surfaces. Pointwise continuous energy cross section data are used, although multigroup data may also be used. Fixed-source adjoint calculations may be made with the multigroup data option. For neutrons, all reactions in a particular cross-section evaluation are accounted for. Both free gas and S(alpha, beta) thermal treatments are used. Criticality sources as well as fixed and surface sources are available. For photons, the code takes account of incoherent and coherent scattering with and without electron binding effects, the possibility of fluorescent emission following photoelectric absorption, and absorption in pair production with local emission of annihilation radiation. A very general source and tally structure is available. The tallies have extensive statistical analysis of convergence. Rapid convergence is enabled by a wide variety of variance reduction methods. Energy ranges are 0-60 MeV for neutrons (data generally only available up to 20 MeV) and 1 keV - 1 GeV for photons and electrons.

As it is known that x-ray photons have an energy range of 100 keV to 1.2 MeV, and copper filter is supposed to be in a regular shape, so all simulations of x-ray interaction with filter matter can be performed using MCNP. This includes the generation of x-ray source spectra, insertion of copper matter, and recording of x-ray detector responses.

The practical guide for the use of MCNP can be found in MCNP manual [LOS93]. The manual includes

- A primer for the novice user;
- The descriptions of the mathematics, data, physics, and Monte Carlo simulation found in MCNP;
- How to prepare input for the code;
- Several examples;
- The explanations of the output; and finally
- How to use MCNP on various computer systems and also details about some of the code internals.

A MCNP application example on x-ray luggage simulation can be found in [XIE95]. A brief introduction is given in Appendix A.

4.3 Design Result

Based on the x-ray source model given in Chapter 3, detector and geometry information of the prototype scanner, the filtered x-ray source spectra at high energy with various thicknesses of copper are obtained to make a final design.

Figure 4.3-1 shows some typical simulation results of the 145 keV energy distribution after attenuation with copper filters varying in thickness from .5 to 1.5 mm. The curves are labeled as $I_{145,\,t}(E)$, where the variable t is the thickness of the copper filter.

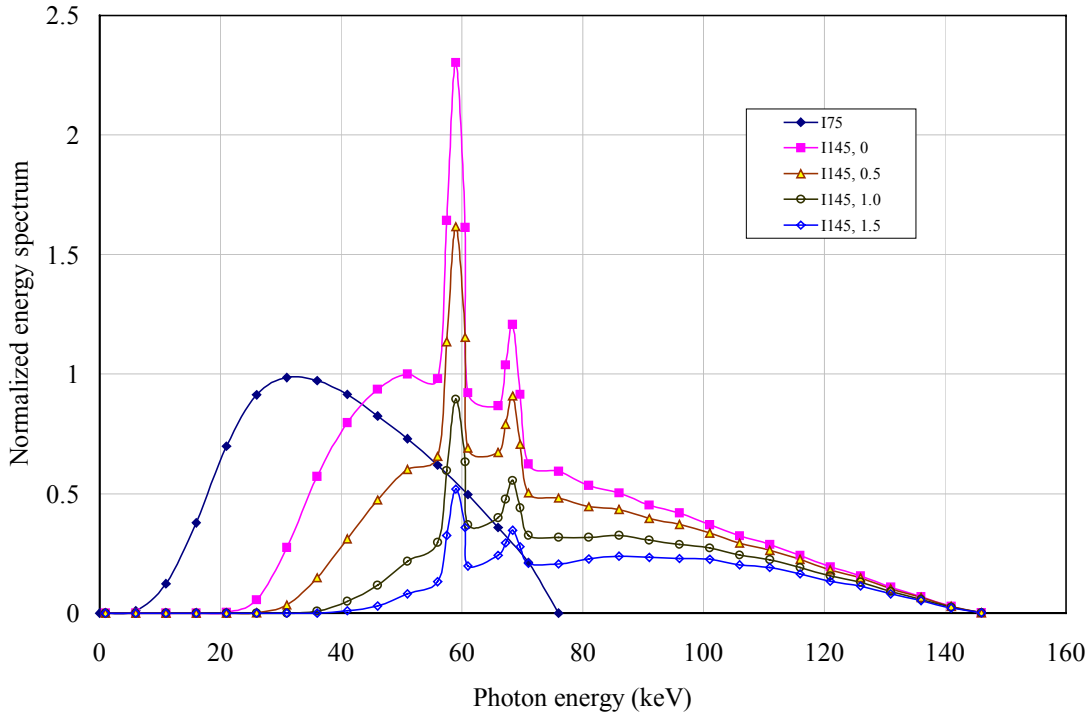

Figure 4.3-1 Simulated x-ray source energy spectra with insertion of the copper filter. Variable t in $I_{145,\,t}$ stands for the thickness of the copper filter.

The output unbalance between high energy and low energy with variation of the copper filter thickness is shown in Figure 4.3-2. It increases monotonically in the range of 0.25 mm to 2.0 mm; while spectrum overlap decrements monotonically in the same range, and is shown in Figure 4.3-3. The cost functions calculated with equal weighting (C_1 = C_2 = 0.5) and a heavier weighting on spectrum overlap (C_1=0.4, C_2=0.6) are given in Figure 4.3-4. Since the amplifier circuit of transmission detector in the prototype scanner is usually not used at its maximum gain, more attention is paid to the spectrum overlap. From these plots the best choice of copper filter thickness is 1 mm, by minimizing the cost function defined in Equation (4.4) when scanning at energy levels of 145 keV and 75 keV and using the heavier weighting on spectrum overlap.

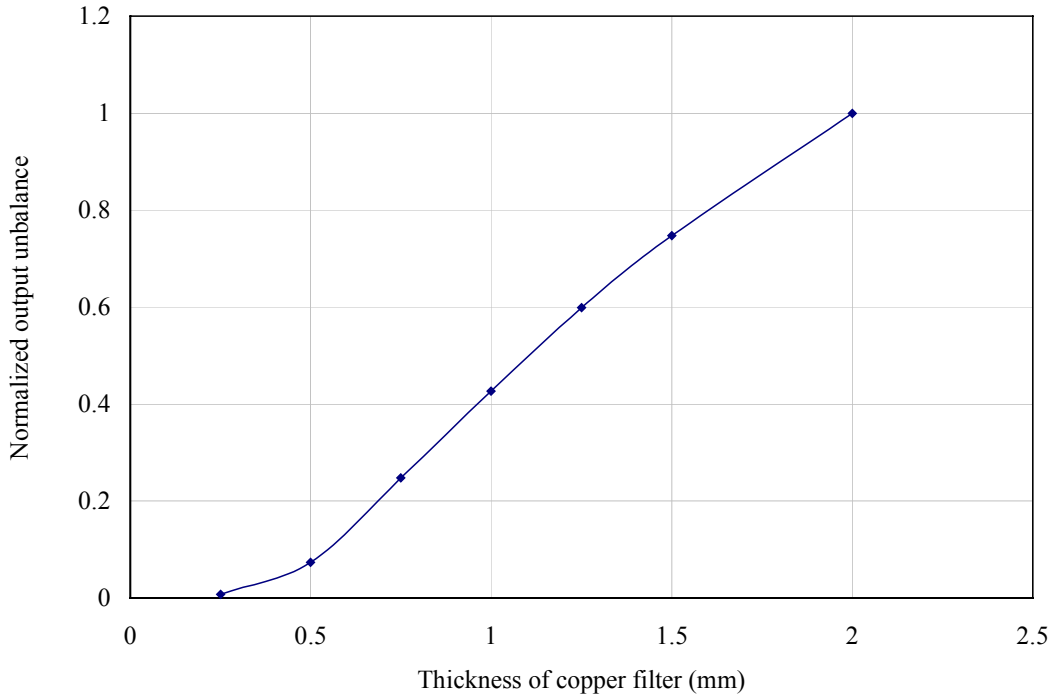

Figure 4.3-2 Unbalance of output signals varying with thickness of copper filter.

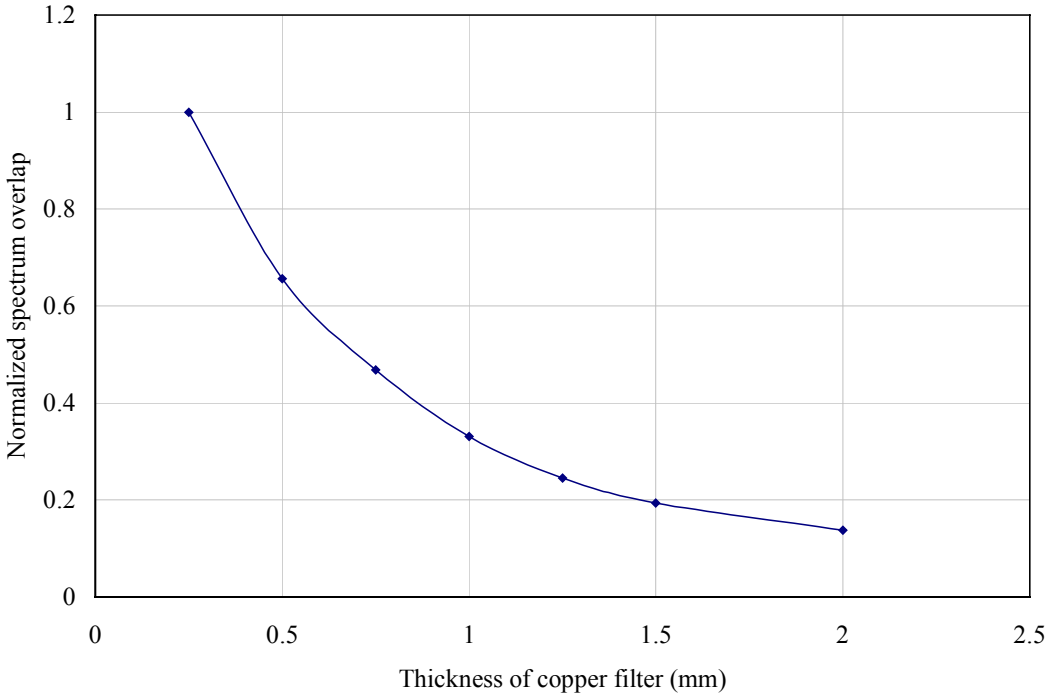

Figure 4.3-3 Spectrum overlap varying with thickness of copper filter.

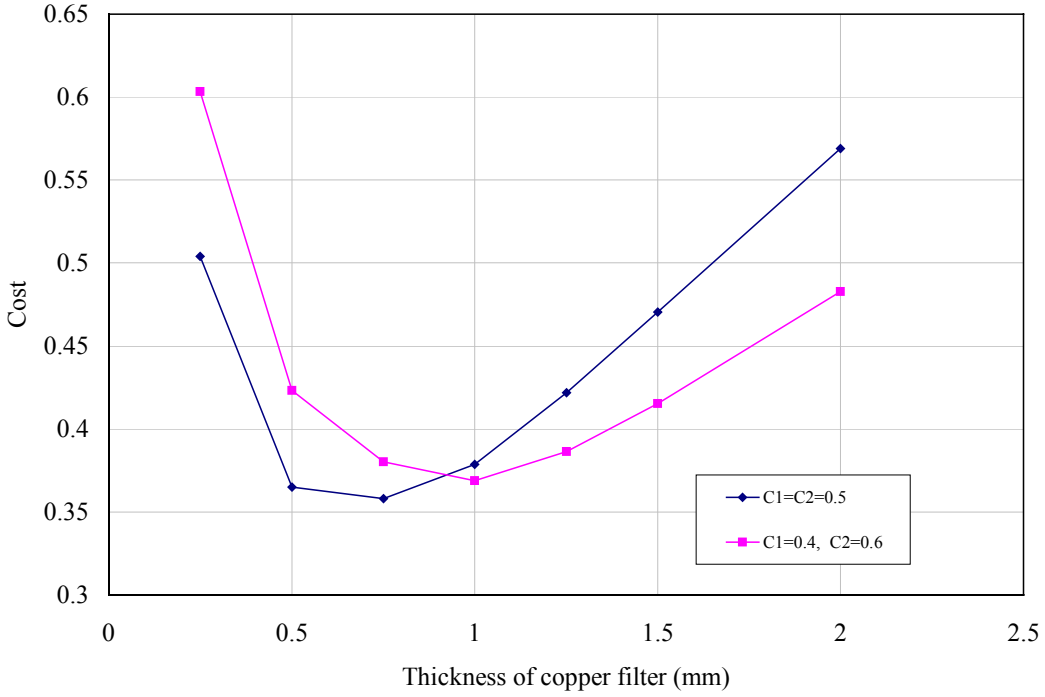

Figure 4.3-4 Cost function varying with thickness of copper filter.

4.4 Evaluation

In this section, we will evaluate the role of the copper filter from two aspects. An imaging example is given to show its role on unbalanced output signals. As for the spectrum overlap, the measurements on two typical materials, an aluminum step wedge (inorganic material) and two plastic step wedges (organic material), will be tabulated with and without the copper filter at x-ray energy of 145 keV. The dual-energy *R* will be calculated to show the difference with and without the copper filter.

4.4.1 Dual-energy measurements on step wedges with and without copper filter

One method to evaluate an algorithm in classification is to observe the derived distances between different classes in a feature space. To verify whether there is any difference with and without the copper filter, transmission images for step wedges (see Figure 4.4-1) were obtained. Tables 4.4-1, 4.4-2, and 4.4-3 show the measurements on three step wedges (aluminum and two plastics) with and without the copper filter. The dual-energy *R* is also calculated.

Figure 4.4-1 Step wedges used in our measurements.

Table 4.4-1 Dual-energy for aluminum step wedge with and without the copper filter.

Thickness (cm)	Normalized transmission signal $G_E = T_E / T_{E0}$ at input energy of E (keV)			Dual energy $R = \log(G_{75})/\log(G_{145})$	
	G_{75}	G_{145} no filter	G_{145} with filter	no filter	with filter
0.26	0.6650	0.8128	0.9353	1.9682	5.9616
0.51	0.5499	0.7130	0.8707	1.7682	4.3907
0.71	0.4887	0.6579	0.8240	1.7098	3.8715
1.01	0.4079	0.5826	0.7610	1.6599	3.4340
1.19	0.3780	0.5479	0.7256	1.6169	3.2463
1.39	0.3518	0.5128	0.6868	1.5643	3.0438
1.52	0.3336	0.4966	0.6643	1.5687	2.9525
2.03	0.2862	0.4336	0.5822	1.4969	2.6900
Mean				1.6691	3.6988
Standard deviation				0.1485	1.0628

Table 4.4-2 Dual energy for white plastic (polyethylene) step wedge with and without the copper filter.

Thickness (cm)	Normalized transmission signal $G_E = T_E / T_{E0}$ at input energy of E (keV)			Dual energy $R = \log(G_{75})/\log(G_{145})$	
	G_{75}	G_{145} no filter	G_{145} with filter	no filter	with filter
0.64	0.8926	0.9226	0.9486	1.4103	2.1520
1.27	0.8100	0.8560	0.8995	1.3548	1.9886
1.91	0.7416	0.7959	0.8519	1.3100	1.8651
2.54	0.6826	0.7411	0.8058	1.2747	1.7691
3.18	0.6283	0.6891	0.7606	1.2482	1.6981
3.81	0.5799	0.6402	0.7214	1.2218	1.6687
4.45	0.5362	0.5937	0.6838	1.1953	1.6396
5.08	0.4961	0.5490	0.6462	1.1689	1.6053
5.72	0.4572	0.5106	0.6101	1.1643	1.5842
6.35	0.4241	0.4773	0.5779	1.1598	1.5642
6.99	0.3934	0.4460	0.5480	1.1552	1.5507
7.62	0.3651	0.4166	0.5180	1.1506	1.5319
8.26	0.3380	0.3881	0.4889	1.1460	1.5158
8.89	0.3144	0.3628	0.4635	1.1415	1.5051
9.53	0.2908	0.3374	0.4382	1.1369	1.4972
Mean				1.2159	1.6757
Standard deviation				0.0860	0.1927

Table 4.4-3 Dual energy for clear plastic (polymethyl methacrylate) step wedge with and without the copper filter.

Thickness (cm)	Normalized transmission signal G_E at input energy of E (keV)			Dual energy $R = \log(G_{75})/\log(G_{145})$	
	G_{75}	G_{145} no filter	G_{145} with filter	no filter	with filter
0.64	0.8680	0.9207	0.9477	1.7137	2.6352
1.27	0.7785	0.8554	0.8967	1.6030	2.2965
1.91	0.7125	0.7999	0.8520	1.5184	2.1173
2.54	0.6493	0.7425	0.8048	1.4504	1.9892
3.18	0.5965	0.6968	0.7640	1.4302	1.9196
3.81	0.5475	0.6514	0.7245	1.4055	1.8692
4.45	0.5032	0.6122	0.6837	1.3998	1.8061
5.08	0.4645	0.5750	0.6492	1.3856	1.7750
5.72	0.4259	0.5386	0.6108	1.3795	1.7312
6.35	0.3967	0.5069	0.5842	1.3611	1.7202
Mean				1.4647	1.9859
Standard deviation				0.1142	0.2917

Let us define $\overline{R_i}$ as the dual-energy mean value for material *i*. From above tables, it can be seen that $\left|\overline{R_j} - \overline{R_k}\right|$ becomes bigger with the copper filter than that is without the copper filter for any two materials *j* and *k* of the three (see Table 4.4-4 and 4.4-5), especially between organic and inorganic materials. That is to say the separation between two types of materials becomes bigger on the average. This result can be explained by mechanism of x-ray interaction with matter, for which x-rays with higher energy have bigger penetration ability than x-rays with lower energy. The copper filter plays a role to filter the x-rays with low energies. The increase in separation contributes to improved accuracy in the detection method in Chapter 5, and finally improves the material characterization.

Table 4.4-4 Separation of dual-energy among three typical materials without the copper filter: $\left|\overline{R_j} - \overline{R_k}\right|$.

	$\overline{R}_{\text{aluminum}}$	$\overline{R}_{\text{clear plastic}}$	$\overline{R}_{\text{white plastic}}$
$\overline{R}_{\text{aluminum}}$	-	0.2044	0.4532
$\overline{R}_{\text{clear plastic}}$	0.2044	-	0.2488
$\overline{R}_{\text{white plastic}}$	0.4532	0.2488	-

Table 4.4-5 Separation of dual-energy among three typical materials with the copper filter: $\left|\overline{R_j} - \overline{R_k}\right|$.

	$\overline{R}_{\text{aluminum}}$	$\overline{R}_{\text{clear plastic}}$	$\overline{R}_{\text{white plastic}}$
$\overline{R}_{\text{aluminum}}$	-	1.7129	2.0231
$\overline{R}_{\text{clear plastic}}$	1.7129	-	0.3102
$\overline{R}_{\text{white plastic}}$	2.0231	0.3102	-

4.4.2 An imaging example with and without copper filter

Dual energy transmission images of a typical piece of luggage were scanned using the prototype scanner. This luggage contained mainly articles of a book, clothing, shoes, hanger, and chocolate. Figure 4.4-2 is the transmission image obtained at the low energy.

Figure 4.4-3 shows two transmission images of the same luggage scanned at high energy. Image 4.4-3a was collected without the copper filter. It is saturated and has a much narrower histogram of pixel values, providing less useful information than image 4.4-3b. The latter was collected after the insertion of the copper filter and is clearer than image 4.4-3a, especially in the lower attenuation objects.

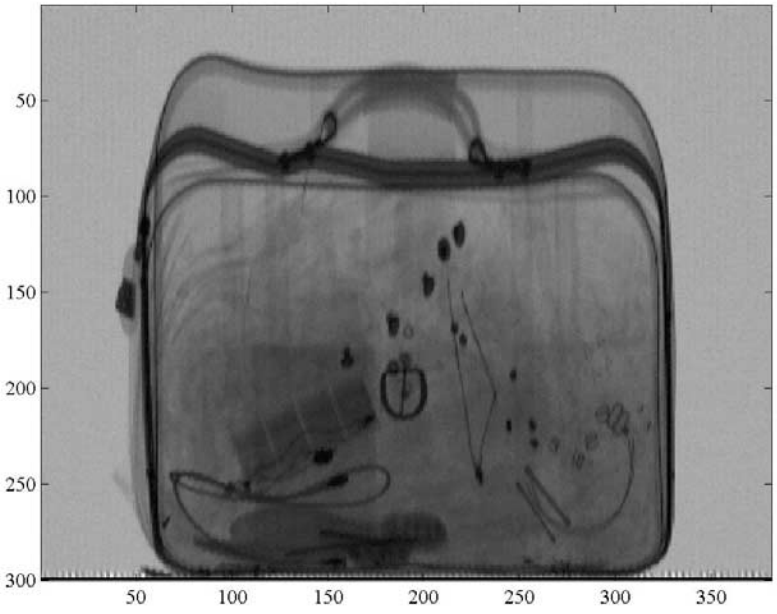

Figure 4.4-2 Transmission image of a typical luggage bag scanned at low energy.

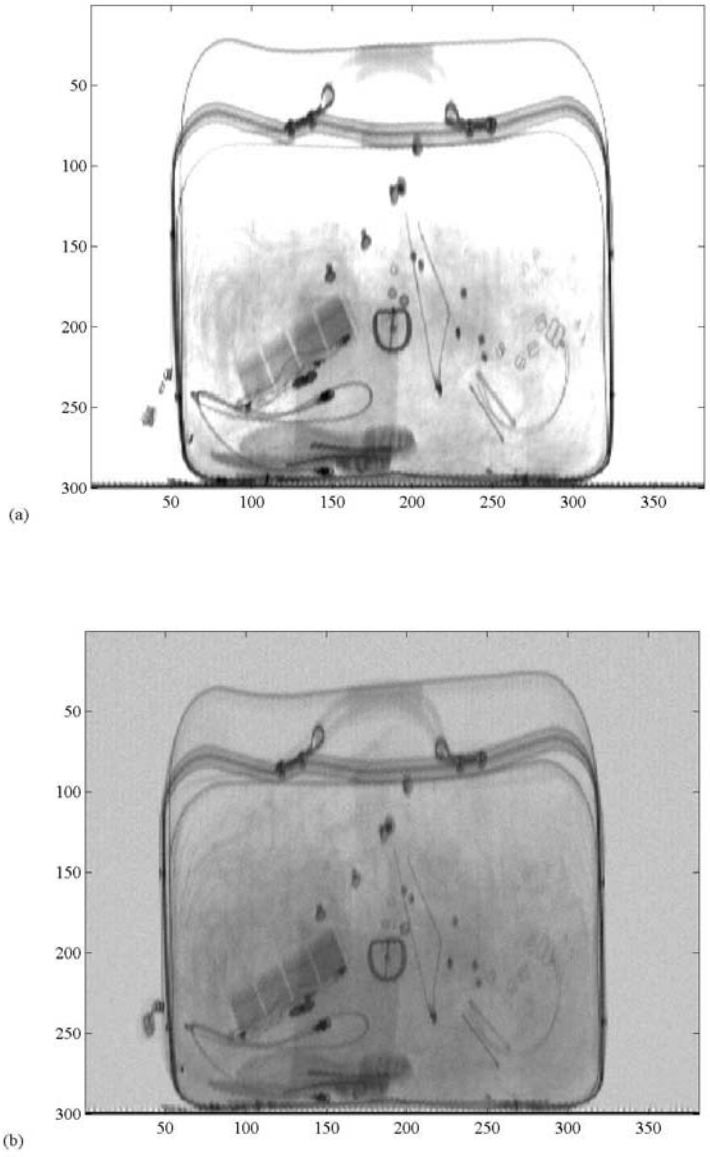

Figure 4.4-3 Transmission images at high energy: (a) without the copper filter, (b) with the copper filter.